JOURNAL OF SOLID STATE CHEMISTRY 105, 112–129 (1993)

Redox Mechanisms and Density of Holes by XAS in the Compensated Series $Bi_{2-x}Pb_xSr_2Ca_{1-x}Y_xCu_2O_{8+\delta}$ ($0 \leq x \leq 1$)

N. MERRIEN, F. STUDER, G. POULLAIN, AND C. MICHEL

CRISMAT, ISMRa, Boulevard du Maréchal Juin, 14050 Caen Cedex, France

AND A. M. FLANK, P. LAGARDE, AND A. FONTAINE

LURE, Bâtiment 209d, Université de Paris-Sud, 91405 Orsay Cedex, France

Received May 26, 1992; accepted November 10, 1992

$Bi_{2-x}Pb_xSr_2Ca_{1-x}Y_xCu_2O_{8+\delta}$ ($0 \leq x \leq 1$) of structural type Bi(2212) is a very interesting solid solution since we are able to adjust the critical temperature over a large range of x by mean of a mere formal exchange of charge between cations which do not belong to the essential $[CuO_2]_\infty$ planes. X-ray absorption spectroscopy was performed at bismuth, lead, and copper L_3-edges on the $Bi_{2-x}Pb_xSr_2Ca_{1-x}Y_xCu_2O_{8+\delta}$ ($0 \leq x \leq 1$) solid solution in order to investigate the formal valence states of the elements and the correlation between hole density on the $[CuO_2]_\infty$ planes and superconducting properties. It is shown that lead substitution does affect the role of the $[BiO]_\infty$ planes which exchange electrons (holes) with the $[CuO_2]_\infty$ planes. The decrease of the hole density in the $[CuO_2]_\infty$ planes with increasing x has been correlated to the decrease of T_c's, whereas the rapid decrease of the diamagnetic volume for $0.3 \leq x \leq 0.7$ has been understood on the basis of a segregation between bismuth- and lead-rich phases.

I. Introduction

Numerous cationic substitutions in the bismuth cuprates have been effected, mainly in the compound $Bi_2Sr_2CaCu_2O_8$, either on the bismuth site by lead, on the strontium site by lanthanum, or on the calcium site by yttrium, in order to modify the number of holes per copper atom in the $[Cu-O_2]_\infty$ planes. Evaluations of the total oxygen content in the bismuth compounds have been made by thermogravimetric analysis (*1*). But to correlate between the hole density and superconducting characteristics such as the critical temperature, a direct evaluation of the hole density is required using spectroscopic methods such as X-ray absorption spectroscopy (XAS) at the L_3 edge of copper.

XAS has been proved to be a valuable tool with which to estimate the formal valence and the electronic state of elements in superconducting oxides (*2–7*). XAS studies of bismuth (*8, 9*) and thallium layered cuprates (*10, 11*) have evidenced a partial reduced valence of the Tl and Bi cations due not to the formation of stable reduced valence states Tl(I) or Bi(I), but more likely to the delocalization of electrons into hybridized band made of 6*s*, 6*p*, and 6*d* levels in the Bi–O or Tl–O plane.

Copper *K*-edge spectroscopy allows a quantitative evaluation of monovalent copper in linear configuration due to a specific transition to nonbonding orbitals ($1s \rightarrow 4p\pi^*$) (Tolentino *et al.* (*12*)). An attempt to go further came from Alp *et al.* (*3*) who tried to correlate the mean edge position to the number of holes. Recently we have shown that, in superconducting thallium cuprates, the mean edge position calculated following the Alp method could be correlated to the

0022-4596/93 $5.00

critical temperature T_c and is thus related to the density of holes, provided the environment of copper is kept constant, as for instance in solid solutions of the type $TlBa_2Ca_{1-x}Y_xCu_2O_{7-\delta}$ (*11*).

Without any hole doping, the cuprates are insulators of the charge transfer type. In other words, the full valence band originates essentially from 2*p* oxygen orbitals but has a 3*d* character. The first empty band above the Fermi level is based on $3d_{x^2-y^2}$ orbitals of Cu: it is the upper Hubbard band, because *U*, the intraatomic Coulomb energy, is much larger than the charge transfer gap. The Cu(II) term is used only to illustrate the charge balance in the chemical formula and represents a simplified and abbreviated label to image the cation Cu(II), described as an admixture of configurations $(\alpha|3d^9\rangle + \beta|3d^{10}\underline{L}\rangle$ with $\alpha^2 + \beta^2 = 1)$ in the presence of itinerant 2*p* holes, which takes place somewhere in the original gap of the undoped cuprate. The $\underline{L}^c$ ligand hole is also an oxygen 2*p* hole but without any itinerant capability; it contributes in the upper Hubbard band.

On an increase in the hole density, a hole impurity-like band is formed at the bottom of the gap, which finally merges with the valence band to build a partially filled conduction band. Thus the stable electronic configuration for these doping holes is the $|3d^9\underline{L}\rangle$ one and the $|3d^8\rangle$ configuration requires a higher energy, as shown by Fujimori *et al.* (*14*), Sawatzki and co-workers (*15*), and Bianconi *et al.* (*16, 17*). Moreover, it has been found that α^2 increases when the hole density increases (*35*).

To check the hole density in the $[CuO_2]_\infty$ planes directly, one can use either $O_{4-x/2+\delta}$ oxygen *K*-edge spectroscopy or Cu L_3-edge spectroscopy. Direct observations of $La_{2-x}Sr_xCuO_{4-x/2+\delta}$ "123" phases and $Bi_2Sr_2CaCu_2O_{8+\delta}$ compounds at the oxygen *K*-edge have shown the dominant oxygen 2*p* character of the conduction band and the strong anisotropy of the hole symmetry in the layered cuprates (*18–22*). Cu L_3-edge spectroscopy is evidently a tool of choice to probe the filling of the *d* band (*23, 24*). The presence of holes is clearly evidenced by an absorption peak due to the $|3d^9\underline{L}\rangle$ configuration. In a recent paper (*13*), the authors have reported a correlation between the hole densities calculated from the $|3d^9\underline{L}\rangle$ intensity and the critical temperatures.

$Bi_2Sr_2CuO_{6+\delta}$, $Bi_2Sr_2CaCu_2O_{8+\delta}$, and $Bi_{1.6}Pb_{0.4}Sr_2Ca_2Cu_3O_{10+\delta}$ are even layered compounds. Two types of XAS experiments have been performed on these compounds and mainly on the 2212 one:

— From the normal stoichiometry, no hole doping can be found in the $[CuO_2]_\infty$ planes. The possibility that the $[Bi–O]_\infty$ planes are an electron reservoir, as suggested first by band structure calculations (*25, 26*), was experimentally evidenced by Retoux *et al.* (*9*) using XAS at the L_3 edge of bismuth. With respect to Bi(III) references (Bi_2O_3, $Bi_2SrNb_2O_9$, and $Bi_2Sr_2CaFe_2O_{10}$), a significant energy shift ($\Delta E \approx 1$ eV) of the superconductor edges toward low energy has been found and interpreted on the basis of extra electrons delocalized in the $[Bi–O]_\infty$ planes. These extra electrons can come from the $[CuO_2]_\infty$ planes, giving rise to self-doping. Holes can also be created by extra oxygens which might be localized in the $[Bi–O]_\infty$ planes. Recent synthesis of bismuth "2212" cuprate under an argon stream by Pham *et al.* (*1*) supports the idea of superconductors without extra oxygen atoms and therefore supports the hypothesis of the electron reservoir.

— Evidence on the oxygen *K*-edge of bismuth "2212" thin films (*22, 27*) has shown that the doping holes are found only in the [*a, b*] plane of the structure; i.e., in the $2p_{x,y}$ orbitals of oxygen.

This work presents results of X-ray absorption spectroscopy of bismuth cuprates $Bi_{2-x}Pb_xCa_{1-x}Y_xCu_2O_{8+\delta}$ ($0 \le x \le 1$) in which bismuth and calcium have been partly substituted by lead and yttrium, respectively. Due to the balance in the substitution, the formal valence of copper is supposed to remain unchanged provided the oxygen stoichiometry is fixed. But magnetic

susceptibility data evidence a decrease of T_c's from 85 to 0 K for $0.2 \leq x \leq 0.6$. In order to check the redox mechanisms in these substituted compounds, we have recorded the Bi L_3- and Pb L_3-edges together with the Cu L_3-edge. Quantitative information about the hole density in the $[Cu-O_2]_\infty$ layers is correlated with T_c. To better understand the change in intensity of the $|3d^9\underline{L}\rangle$ line at the Cu L_3-edges of $Bi_2Sr_2CaCu_2O_{8+\delta}$ sinters, a comparison with polarized spectra of oriented Bi(2212) thin film has been undertaken.

II. Experimental

Bismuth-based and bismuth–lead-based compounds were prepared by reacting appropriate amounts of Bi_2O_3, PbO, Y_2O_3, and CuO with $SrCO_3$ and $CaCO_3$. The mixtures were ground, pressed into pellets, and heated in air at 800°C for 12 hr and then at 865°C for 16 hr. Final materials were checked by X-ray powder diffraction for purity and superconducting properties were studied by ac susceptibility measurements (Fig. 1).

Lanthanum cuprate, $La_2CuO_{4-\delta}$, was prepared from the oxides La_2O_3 and CuO, mixed and heated in air in a platinum crucible. TGA analysis of the final product has shown δ to be less than ± 0.02.

$La_2Cu_{0.5}Li_{0.5}O_{4-\delta}$ was synthesized from a mixture of the oxides La_2O_3 and CuO and of lithium carbonate Li_2CO_3 according to the work of Attfield and Férey (*28*). The preparation was pelletized, heated in flowing oxygen at 900°C for 12 hr and cooled to room temperature at the rate of 50°C/hr. TGA analysis could not be performed on this sample due to possible lithium loss during reduction. Iodometric titration confirmed the presence of trivalent copper and led to a δ value close to 0.04.

Final materials were checked by X-ray and electron diffraction for purity and defect density. Superconducting properties were studied by resistivity and susceptibility measurements on the same small bars. The results of the synthesis, structure determinations, and physical properties of these compounds have been published elsewhere (*29, 30*). Thin films of $Bi_2Sr_2CaCu_2O_8$ have been prepared on monocrystalline (100) MgO substrates using a laser ablation method with postannealing treatment following a method described by Brousse *et al.* (*31*).

The XAS spectra at the Pb (13035 eV) and Bi (13419 eV) L_3-edges were recorded at room temperature on powder samples in transmission mode. The experiments were performed at LURE (ORSAY) using the synchrotron radiation from the DCI storage ring operated at 1.85 GeV with a nominal current of 250 mA. X-rays were monochromatized by a Si (331) channel cut and the incident and transmitted intensities were measured using two ionization chambers. The energy resolution was estimated to be better than 1.6 eV at the Bi and Pb L_3-edges, whereas the reproducibility of the energy position of the spectral features is close to 0.3 eV.

The normalization procedure used throughout this work was a standard one: after substraction of the same background out of the XANES and EXAFS spectra, recorded in the same experimental conditions, a point located at an energy of 800 eV from the edge, where no more EXAFS oscillations were still observable, was set to unity.

The XAS spectra at the Cu L_3-edge (931.2 eV for the $|3d^9\rangle$ transition) were also recorded at room temperature on powder samples by a total electron yield method. The experiments were performed using the synchrotron radiation from the super ACO ring operated at 800 MeV with a typical current of 250 mA. The X-rays were monochromatized by two beryl crystals (1010) and the electrons ejected from the samples were accelerated toward a channeltron electron multiplier perpendicular to the beam line. The thickness of the probed upper layer is given by the average electron escape depth of all emitted electrons with an energy spectrum extending from a maximum at 2–4 eV,

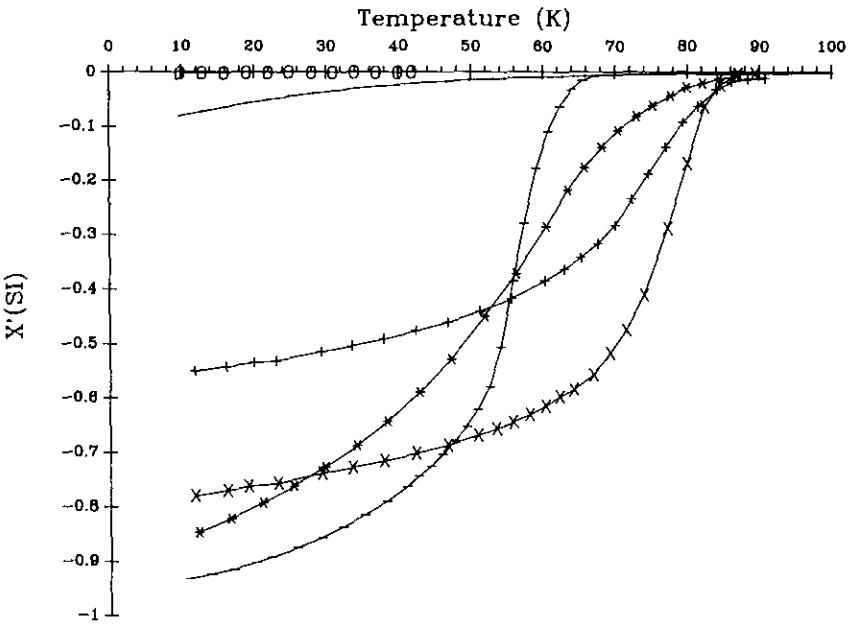

FIG. 1. Normalized real part of the magnetic susceptibility as a function of temperature for the $Bi_{2-x}Pb_xCa_{1-x}Y_xCu_2O_{8+\delta}$ series: (x x x) $x = 0$; (+ + +) $x = 0.1$; (* * *) $x = 0.2$; (– – –) $x = 0.3$; (———) $x = 0.5$; (○ ○ ○) $x = 0.75$.

due to secondary electrons, to the energy of direct valence-band photoemitted electrons with kinetic energy $h\nu$-ϕ, where ϕ is the metal work function. Because the mean free path is a maximum for the low-energy secondary electrons, which are more numerous than the direct photoelectrons and Auger electrons, the average thickness determined by the electron escape depth of secondary electrons is about 100–200 Å. In order to get rid as much grain surface contamination as possible, fresh synthesized pellets of each composition were thoroughly ground before being spread on a sticky band and put immediately under vacuum for the measurements. The energy resolution was estimated to be better than 0.8 eV, whereas the reproducibility of the energy position feature is close to 0.1 eV. The top of the $|3d^9\rangle$ transition for all the compounds has been set to a common value chosen arbitrarily and the spectra have been least-squares fitted by a combination of Gaussian and Lorentzian shapes in order to obtain the relative intensities of the transitions.

III. Results

A. Bismuth L_3-Edge

1. Reference Compounds

Structure. The low-temperature monoclinic form of the bismuth oxide Bi_2O_3, which contains Bi(III) formally, has a complex and unique structure in which Bi atoms occupy two types of irregular coordination polyhedra. The first environment of Bi atom has five oxygen nearest neighbors at the vertices of a distorted octahedron at distances ranging from 2.08 to 2.63 Å (and a sixth at 3.25 Å) while the second type has an octahedral arrangement of six oxygen nearest neighbors at distances ranging from 2.14 to 2.80 Å; three of those are closer to the Bi cation (2.14–2.29 Å) than the other three (2.48–2.80 Å).

Another compound, $Bi_2SrNb_2O_9$ has been chosen as a reference for Bi(III). Its structure is an overgrowth of $[Bi_2O_2]$ layers, in which the metal atom is bonded to four oxygen atoms arranged in a regular square on one side of it, with the lone $6s^2$ pair of the

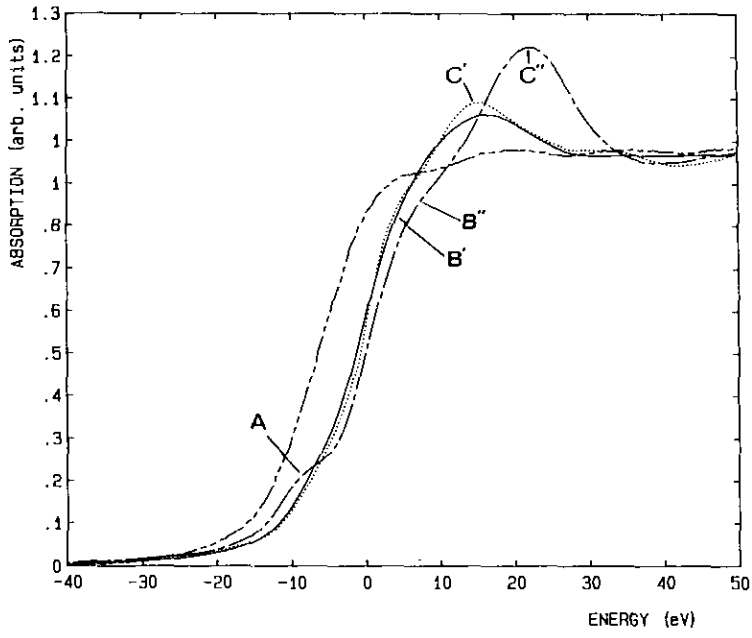

FIG. 2. Bismuth L_3-edges of some reference compounds: (__ - - __) metallic bismuth; (———) Bi_2O_3; (__ · __) $NaBiO_3$; (· · ·) $Bi_2SrNb_2O_9$.

Bi(III) electrons occupying the apex of the tetragonal pyramid (4 × 2.8 Å), and double perovskite layers [$SrNb_2O_9$]. This arrangement of bismuth has been proposed by several authors for the double Bi–O layers in the superconducting compounds.

$NaBiO_3$, the reference for Bi(V), presents an ilmenite structure with the bismuth atoms in a regular oxygen octahedron (Bi–O = 1.91 Å).

XAS spectra. The selection rules for the photoelectric excitation in the dipolar approximation allow only the final states with a symmetry L_f differing from the initial state L_i by ± 1. Thus, at the L_3-edge, not only the 6*d* states are accessible but also the 6*s* states if empty.

XANES spectra of the reference compounds $NaBiO_3$, Bi_2O_3, $Bi_2Sr_2Nb_2O_9$, and metallic bismuth have been recorded at the Bi L_3-edge. As displayed in Fig. 2, there exist energy shifts between $NaBiO_3$ [Bi(V)] and Bi_2O_3[Bi(III)] on one hand, and between Bi_2O_3 and metallic bismuth on the other. As expected, the edge energies, taken at the midpoint of the main slope of the curves, increase with increasing valence state of bismuth (Table I). This effect results both from the increase of the relaxation energy induced by the core hole in the final state and from the decrease of the bond lengths which push the antibonding molecular orbitals to higher energies.

The prepeak A exists only in the $NaBiO_3$ spectrum (Fig. 2). It reflects the $2p_{3/2} \rightarrow 6s$ transition, since the 6*s* levels are vacant in Bi(V). Such a prepeak characteristic of the absence of the lone pair doublet allows unambiguous determination of the highest valence state and thus discrimination between Bi(III) and Bi(V). Following Rao and Wong (*37*), who measured the Pb L_3-edge of octahedral lead in PbO_2, the peaks B′, C′ and B″, C″ for Bi_2O_3 and $NaBiO_3$, respectively, can be assigned to some specific transitions using the molecular orbital approach, which explains the splitting of the 6*d* states into nonbonding orbitals (t_{2g}) and antibonding ones (e_g):

— A: $2p_{3/2} \rightarrow 6s$
— B: $2p_{3/2} \rightarrow 6d(t_{2g})$
— C: $2p_{3/2} \rightarrow 6d(e_g)$.

TABLE I

SIMULATION PARAMETERS OF THE COPPER L_3-EDGES FOR REFERENCE COMPOUNDS AND SUPERCONDUCTING CUPRATES OF THE $Bi_{2-x}Pb_xCa_{1-x}Y_xCu_2O_{8+\delta}$ ($0 \le x \le 1$) SERIES

Compounds		$\|3d^9\rangle$	$\|3d^9\underline{L}\rangle$	$n_h = I/(I + I_0)$	$n_{x,y}$	T_c (K)
La_2CuO_4	E	931.1	*	*	*	**
	Γ	0.53				
$La_2Li_{0.5}Cu_{0.5}O_4$	E	931.1	933.45	0.84	***	**
	Γ	0.46	0.47			
$Bi_2Sr_2CaCu_2O_{8+\delta}$, thin film 0°	E	931.4	932.8	0.19	0.19	85
	Γ	0.60	0.95			
$Bi_2Sr_2CaCu_2O_{8+\delta}$, thin film 35°	E	931.3	932.6	0.16	0.19	85
	Γ	0.60	0.95			
$Bi_2Sr_2CaCu_2O_{8+\delta}$, thin film 75°	E	930.9	*	*	*	85
	Γ	0.59				
$Bi_2Sr_2CaCu_2O_{8+\delta}$, powder	E	931.3	932.4	0.15	0.18	84
	Γ	0.66	0.9			
$Bi_{1.9}Pb_{0.1}Sr_2Ca_{0.9}Y_{0.1}Cu_2O_{8+\delta}$, powder	E	931.3	932.5	0.14	0.165	85
	Γ	0.67	0.9			
$Bi_{1.8}Pb_{0.2}Sr_2Ca_{0.8}Y_{0.2}Cu_2O_{8+\delta}$, powder	E	931.3	932.6	0.13	0.155	78
	Γ	0.67	0.8			
$Bi_{1.7}Pb_{0.3}Sr_2Ca_{0.7}Y_{0.3}Cu_2O_{8+\delta}$, powder	E	931.3	932.6	0.10	0.12	62
	Γ	0.67	0.9			
$Bi_{1.5}Pb_{0.5}Sr_2Ca_{0.5}Y_{0.5}Cu_2O_{8+\delta}$, powder	E	931.3	932.6	0.07	0.085	40
	Γ	0.64	0.9			
$Bi_{1.25}Pb_{0.75}Sr_2Ca_{0.25}Y_{0.75}Cu_2O_{8+\delta}$, powder	E	931.3	*	<0.04	<0.05	**
	Γ	0.61				
$BiPbSr_2YCu_2O_{8+\delta}$, powder	E	931.3	*	0	0	**
	Γ	0.55				

Note. In order to properly compare the $|3d^9\underline{L}\rangle$ line intensities, the linewidths of this transition have been kept constant and fixed to 0.9 eV. E and Γ are respectively the energy and linewidths of the lines. * Not detectable $|3d^9\underline{L}\rangle$ line. ** Not superconducting. *** Polarization dependence not known.

Qualitatively the location of these electronic transitions obeys the so-called $(E-E_0)R^2$ = const. rule (*32*), quantitatively valid only in case of wide bands: the antibonding transition for longer distances arises at lower energies (Table I).

In PbO_2, the analysis of XAS can be as simple as presented above since the crystal field is purely octahedral. It is quite clear that if one of the oxygen neighbors moves to infinity, the e_g orbitals shift to lower energy and can merge with the B peak.

2-Bismuth Cuprates

The Bi L_3 XANES spectra for some x values of the $Bi_{2-x}Pb_xSr_2Ca_{1-x}Y_xCu_2O_{8-\delta}$ series are presented in Fig. 3 with three reference compounds: Bi metal, $NaBiO_3$, and Bi_2O_3. As observed previously in the spectra of 2201, 2212, and 2223 superconductors (*9*), there is a shift of the lead-substituted bismuth cuprates toward lower energies with respect to Bi_2O_3. We can see that the shift increases with replacement of bismuth by lead (Fig. 3, inset). A similar observation can be made for the Bi L_3 XANES spectrum of $Bi_{1.4}Pb_{0.6}Sr_2Ca_2Cu_3O_{10+\delta}$ (Bi 2223) (Fig. 4) which exhibits an energy shift similar to that of the $x = 0.5$ term of the series. A small shoulder also appears at the same energy as prepeak A in $NaBiO_3$. This feature, which corresponds to partially empty 6*s* levels, lead us to the conclusion that some amounts of Bi(VI) (less than 10%) are present in the

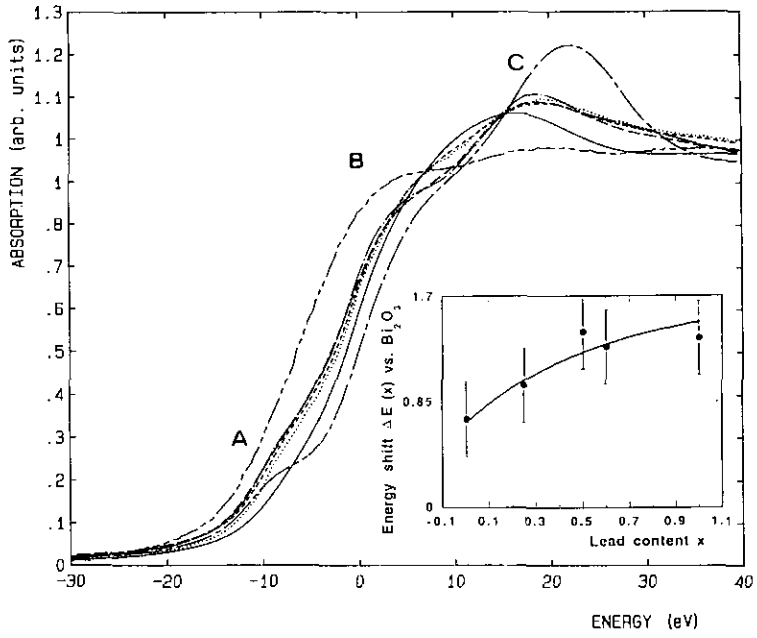

FIG. 3. Bismuth L_3-edges of some compounds of the $Bi_{2-x}Pb_xCa_{1-x}Y_xCu_2O_{8+\delta}$ series: (__ - - __) metallic bismuth; (———) Bi_2O_3; (__ - __) $NaBiO_3$; (· · ·) $x = 0$; (- - -) $x = 0.25$; (– – –) $x = 0.5$; (— · —) $x = 1$. Inset: Variations of the energy shift with respect to Bi_2O_3 of Bi L_3-edges as a function of lead content.

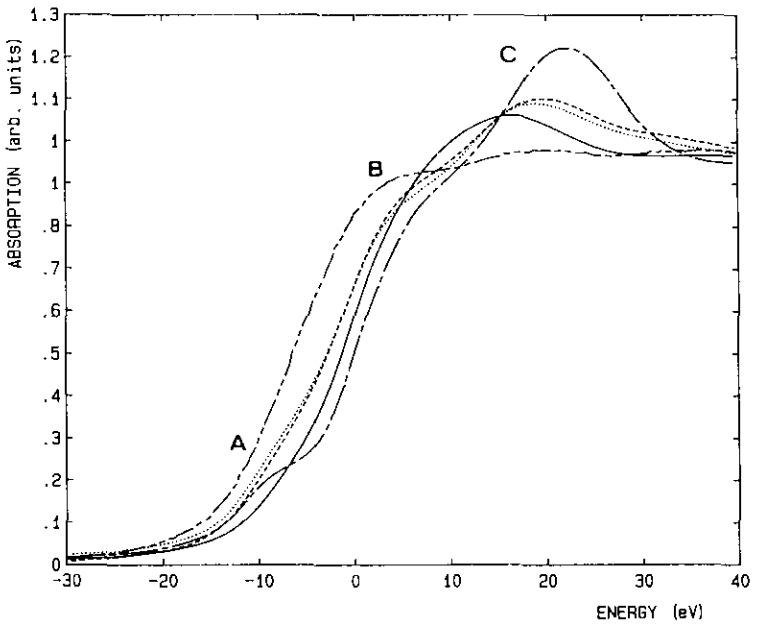

FIG. 4. Bismuth L_3-edges of the same reference compounds and (· · ·) $Bi_{1.5}Pb_{0.5}Sr_2Ca_{0.5}Y_{0.5}Cu_2O_{8+\delta}$; (- - -) $Bi_{1.4}Pb_{0.6}Sr_2Ca_2Cu_3O_{10+\delta}$.

Bi–O layers of these compounds. We use the Bi(V) concept for superconductors to simplify the vocabulary. What XAS evidences is only the creation of holes in the 6*s* bands. It obviously has a real meaning of valency for $NaBiO_3$ which is an insulator. For superconductors, which are metals at room temperature, one should speak of overlap of the 6*s* bands and the 6*d* ones which are probed by the L_3 spectroscopy.

Thus, at the Bi L_3-edge, the bismuth-substituted cuprates present a unique feature which can be described as the simultaneous presence of two oxidation states of bismuth in different concentrations: one state smaller than 3, in a larger amount than the other one, the Bi(V) state, whose presence appears only as a small shoulder.

The formal valency of bismuth lower than 3 in the nonsubstituted bismuth cuprates ("2201," "2212," and "2223" compounds) has been interpreted by Retoux *et al.* (*9*) as follows: in the rock salt-type layers, the very anisotropic crystal field around the bismuth atoms leads to the splitting of the 6*p* levels. The resulting decrease in energy of some 6*p* orbitals and their hybridization with 6*s* levels induce a σ (Bi6s–6$p_{x,y}$–O2$p_{x,y}$) band by overlapping with the oxygen $2p_{x,y}$ levels in the Bi–O layers. This bond seems to be responsible for the stabilization of some extra electrons on the bismuth cations but also for the creation of some density of holes in a dominantly 6*s* hybridized level which can account for the small intensity of the A bump. The necessary large distortions of the oxygen polyhedra around bismuth could be created by the way of the Bi–O layers modulations.

We can see that the shift towards low energies of the substituted compounds increases when the substitution rate x increases for $0 \leq x \leq 0.5$. Simultaneously, the B peak, which is connected to the long Bi–O distances, moves towards low energy; i.e., these long Bi–O distances tend to increase again. This appears clearly from the Bi L_3-edges of $x = 0.5$ and $x = 1$ compounds (Fig. 3) on which the B and C lines are much more separated than for the lead poor compounds. Of course, this is the antibonding e_g ($6d_{x^2-y^2}$) part of the B peak, which is pushed toward lower energy when the long Bi–O distances increase.

Both features are consistent with a concentration of the extra electrons on the bismuth sites in the $[Bi–O]_\infty$ layers when the lead content increases.

B. Lead L_3-Edge

1. Reference Compounds

Structure. The so-called yellow PbO, the reference for the Pb(II) state, has an orthorhombic cell in which the metal atom is bonded to four oxygen atoms arranged in a rhombic distorted square on one side of it, with the lone $6s^2$ pair of the Pb(II) electrons occupying the apex of the tetragonal pyramid. In this geometry, the Pb–O distances are split between two short (2.20 Å) and two long (2.49 Å) ones.

In contrast, lead dioxide, PbO_2, has the rutile structure in which the mean Pb(IV)–O distance of lead to the six neighbors of the octahedra is close to 2.18 Å, within 0.01 Å.

The mixed valence oxide Pb_3O_4 crystallizes in a tetragonal cell in which lead is present under two valence states, Pb(IV) and Pb(II). Pb(IV) ions occupy the center of the slightly distorted octahedra (Pb(IV)–O distances close to 2.13 Å and 2.20 Å) whereas Pb(II) coordination polyhedra are square base pyramids (Pb(II)–O distances ranging from 2.21 Å in the plane to 2.64 Å for the apical oxygen).

L_3-edge. The selection rules are the same as for the bismuth L_3-edge and the core hole width is 5.8 eV. XANES spectra have been recorded at the Pb L_3-edge for the three reference compounds (Fig. 5); PbO, PbO_2, and Pb_3O_4, whose spectrum appears always between the two other ones, as expected for a mixed valence compound, and can be simulated by a linear combination of PbO and PbO_2 spectra: 0.7 PbO + 0.3 PbO_2.

Like the $NaBiO_3$ spectrum, the PbO_2

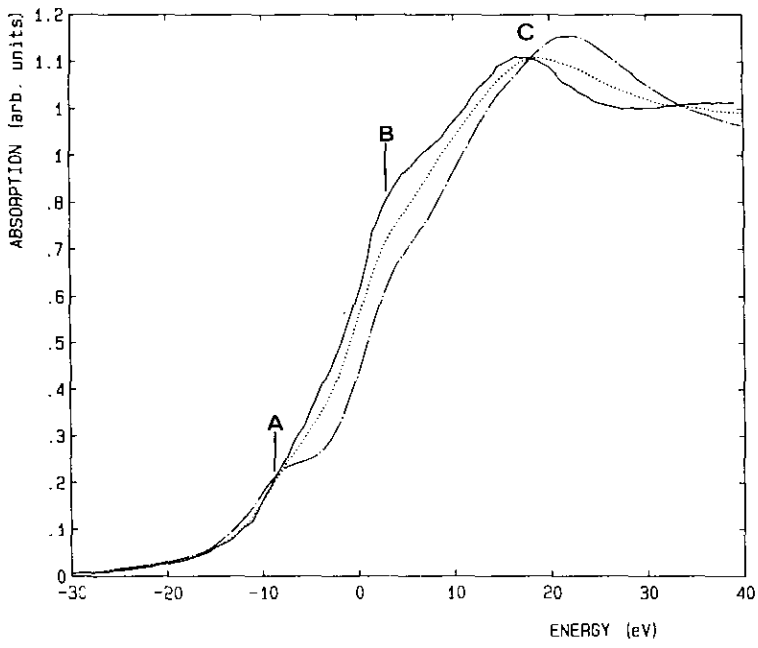

FIG. 5. Lead L_3-edges for the reference compounds (———) PbO, (· · ·) Pb_3O_4, and (__ · __) PbO_2.

spectrum clearly exhibits the low energy shoulder (A on Fig. 4) due to the $2p_{3/2} \rightarrow 6s$ transition, whereas the B ($2p_{3/2} \rightarrow 6d$ (t_{2g})) and C ($2p_{3/2} \rightarrow 6d$ (e_g)) transitions appear at higher energies than for PbO, in agreement with the longer Pb–O distances.

Again, in the PbO spectrum (Fig. 5), one cannot exclude a mixed contribution of $6d$ (t_{2g}) and $6d$ (e_g) orbitals in the B peak induced by the distorted oxygen polyhedra around lead.

2. *Bismuth Cuprates*

The Pb L_3 XANES spectra of the $Bi_{2-x}Pb_xSr_2Ca_{1-x}Y_xCu_2O_{8+\delta}$ ($x = 0.25$, $x = 0.5$, $x = 0.75$, and $x = 1$) series (Fig. 6) and of the $Bi_{1.6}Pb_{1.4}Sr_2Ca_2Cu_3O_{10+\delta}$ cuprate (Bi 2223: Fig. 7) are shown with the reference compounds (PbO, PbO_2) and the $x = 0.5$ term of the series in order to visualize the shift of the lead-substituted bismuth cuprate edges.

Bearing in mind the small lead content of our compounds, the signal to noise ratio decreases with x so that the spectra for the lowest x values ($x = 0.25$ and 0.5) look rather noisy. Nevertheless, three points are in favor of a mixed valence of lead in the studied solid solution:

— The presence of a low energy shoulder corresponding to the A peak of PbO_2 which clearly indicates that holes are dense in the lead $6s$ levels. This peak looks more pronounced for the lowest x values.

— A shift of the edges of the cuprates, taken at midheight of the main absorption line, toward high energy with respect to the main absorption line of PbO. Taking into account the experimental resolution, this shift of the cuprates toward high energy appears to decrease also with increasing x values and to nearly vanish for $x \geq 0.75$ (Fig. 5, inset). This last result indicates that at high lead content the valence of lead is fixed as Pb(II) and is mixed, Pb(II)/Pb(IV), for low lead content.

— A shift of the main peak corresponding to the C transition ($2p_{3/2} \rightarrow 6d$ (e_g)) toward higher energies with respect to PbO indicat-

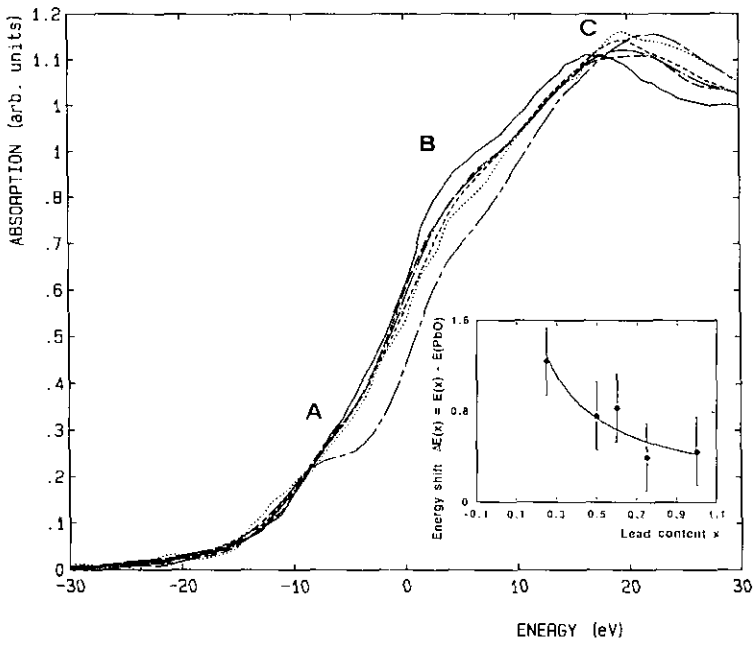

FIG. 6. Lead L_3-edges for the reference PbO, PbO_2, and some compositions of the $Bi_{2-x}Pb_xCa_{1-x}Y_xCu_2O_{8+\delta}$ series: (———) PbO; (__ - __) PbO_2; (· · ·) $x = 0.25$; (- - -) $x = 0.5$; (– – –) $x = 0.75$; (__ · __) $x = 1$. Inset: Variations of the energy shift with respect to PbO of Pb L_3-edges as a function of lead content.

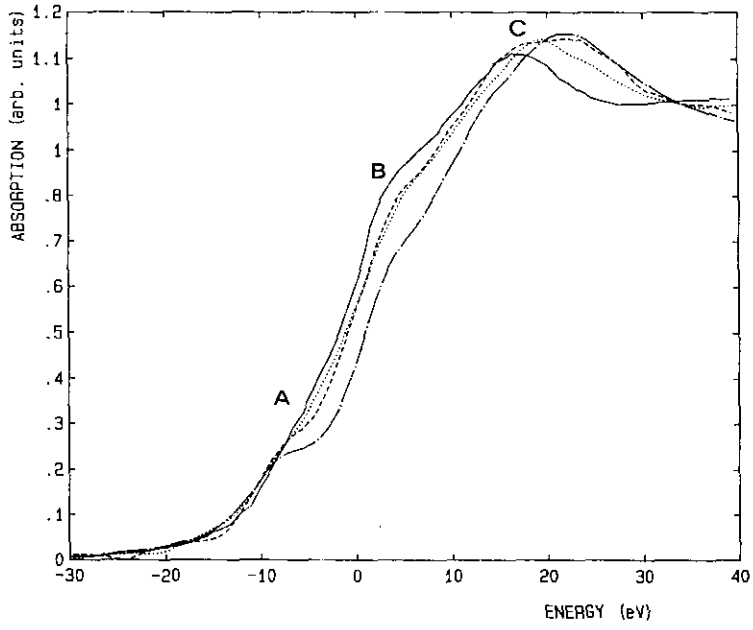

FIG. 7. Lead L_3-edges for the same reference compounds and (———) PbO, (__ · __) PbO_2, (· · ·) $Bi_{1.5}Pb_{0.5}Sr_2Ca_{0.5}Y_{0.5}Cu_2O_{8+\delta}$, and (- - -) $Bi_{1.4}Pb_{0.6}Sr_2Ca_2Cu_3O_{10+\delta}$.

ing a decrease of the shortest Pb–O distances in the cuprates, in agreement with an increase of the mean valence state of lead.

As a conclusion of this work at the Bi and Pb L_3-edges, one can say that the valence state of bismuth appears to be less than III, whereas the valence state of lead is more than II. The first point confirms previous observations (*9*) and was interpreted in the $Bi_2Sr_2CaCu_2O_8$ compound as the result of electron transfer from $[CuO_2]_\infty$ to $[BiO]_\infty$ planes.

The mixed valence state of lead is more unusual since Pb(II) is dominant in the Cava phase, Pb(IV) in $(Tl_{0.5}Pb_{0.5})Sr_2Ca_{n-1}Cu_nO_{2n+3}$, and yet no mixed valence state of lead has been observed in the superconducting layered cuprates. To explain such a result one can assume that a transfer of some electrons takes place between the $[CuO_2]_\infty$ and the $[BiO]_\infty$ planes and/or inside the latter planes between lead and bismuth cations.

C. The Copper L_3-Edge and the Hole Density

1. References

Structure. In nonsuperconducting La_2CuO_4, the octahedral coordination of copper(II) is the result of an intergrowth between single rock salt $[LaO]_\infty$ layers and single perovskite $[LaCuO_3]_\infty$ layers; nevertheless, due to the Jahn-Teller effect, a strong distortion of the CuO_6 octahedra occurs which stabilizes long Cu–O distances along the **c** axis ($2 \times d_{Cu-O} \approx 2.40$ Å) and short distances in the basal planes ($4 \times d_{Cu-O} \approx 1.98$ Å).

The reference for Cu(III) species, $La_2Li_{0.5}Cu_{0.5}O_{4-\delta}$, is a K_2NiF_4-type oxide synthesized for the first time under high pressure (*36*). In this stoichiometric phase, Cu and Li cations are distributed into distorted octahedral sites. The chemical analysis of the latter oxide showed in fact a mixed valency of copper with 85% of Cu(III) and 15% Cu(II) suggesting oxygen deficiency.

L_3-Edge. Copper L_3-edge spectra of cuprates La_2CuO_4 and $La_2Li_{0.5}Cu_{0.5}O_{3.96}$ taken as references for Cu(II) and Cu(III) valence states, respectively, are shown in Fig. 8 together with the fitted curves.

The spectrum of the first compound is characterized by one peak centered around 931.2 eV and of 0.53 eV for HWHM; the results of the simulation are presented in Table I. This single peak corresponds to the transition $|2p_{3/2}\ 3d^9\rangle \rightarrow |\underline{2p}\ 3d^{10}\rangle$, giving rise to the copper final state $[1s^22s^22p^53s^23p^63d^{10}4s^04p^0]$.

The spectrum of $La_2Li_{0.5}Cu_{0.5}O_{3.96}$ exhibits two peaks, clearly visible due to their large energy difference. The intensity of the second peak at $E_1 = 933.45$ eV (Table I) is much larger than the other one at $E_0 = 931.1$, keeping the same HWHM linewidths. The energy of the first peak is close to the values found for the Cu(II) reference La_2CuO_4 and thus corresponds to the same transition $|2p_{3/2}\ 3d^9\rangle \rightarrow |\underline{2p}\ 3d^{10}\rangle$, attesting for the presence of the Cu(II) valence state in a small amount. The second peak, as shown in previous papers (Bianconi *et al.* (*16*)), is due to the $|2p_{3/2}\ 3d^9\underline{L}\rangle \rightarrow |\underline{2p}\ 3d^{10}\underline{L}\rangle$ transitions.

From the intensities of both peaks I_0 and I_1, one can deduce a mean density of holes per copper

$$n_h = \frac{I_{|3d^9\underline{L}\rangle}}{I_{|3d^9\rangle} + I_{|3d^9\underline{L}\rangle}} = 0.85$$

in good agreement with the chemical analysis. It is worth noting here that, in the charge transfer model, the hole density in the $2p_{x,y}$ oxygen band should only be 0.425 due to the small copper concentration in this cuprates.

2. Bismuth Cuprates

Five compositions of the solid solution $Bi_{2-x}Pb_xSr_2Ca_{1-x}Y_xCu_2O_{8+\delta}$ corresponding to $x = 0$, $x = 0.1$, $x = 0.2$, $x = 0.3$, $x = 0.5$, $x = 0.75$, and $x = 1$ have been studied by X-ray absorption spectroscopy at the Cu L_3-edge.

The intensity of the $|3d^9\underline{L}\rangle$ shoulder starts to be rather constant for $x \leq 0.2$ and then decreases when x increases (Fig. 9). For the determination of the line intensities, we

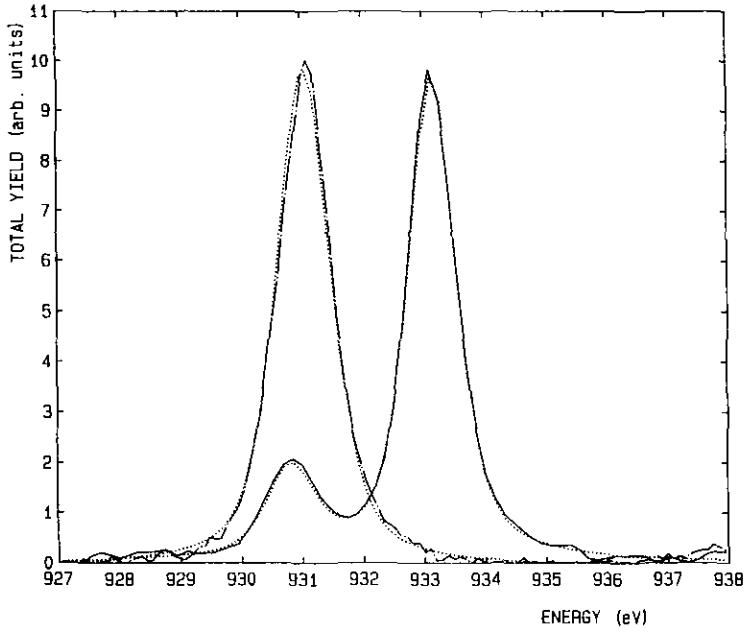

FIG. 8. Copper L_3-edges of two compounds used as references: (__ · __) La_2CuO_4 for Cu(II) formal valence, (———) $La_2Li_{0.5}Cu_{0.5}O_{3.96}$ for Cu(III) formal valence, and (· · ·) fitted curves.

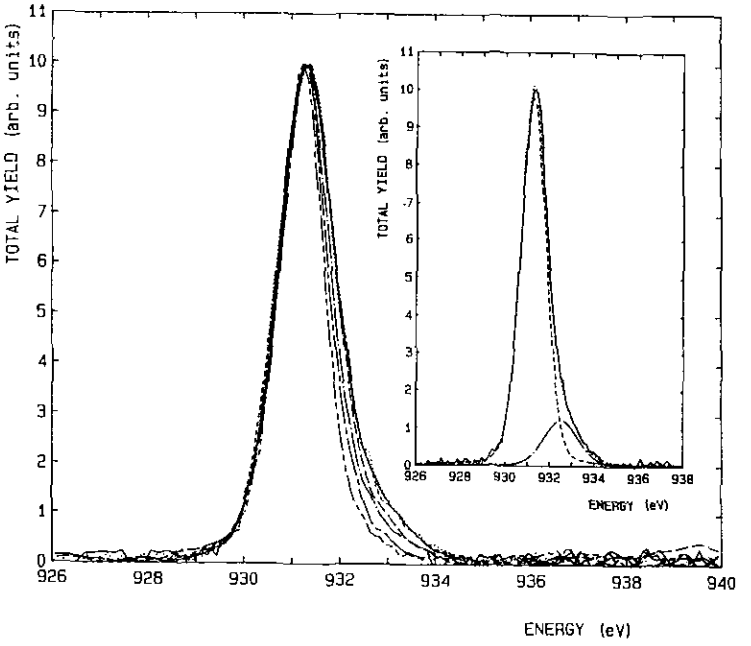

FIG. 9. Copper L_3-edges for the $Bi_{2-x}Pb_xCa_{1-x}Y_xCu_2O_{8+\delta}$ series: (———) $x = 0$; (· · ·) $x = 0.1$; (- - -) $x = 0.2$; (– – –) $x = 0.3$; (__ · __) $x = 0.5$; (__ - __) $x = 0.75$; (__ -- __) $x = 1$. Inset: Simulation curves for the $Bi_{1.9}Pb_{0.1}Sr_2Ca_{0.9}Y_{0.1}Cu_2O_{8+\delta}$ compound: (———) experimental; (· · ·) total fit; (- - -) $|\underline{2p}3d^9\rangle$ final electronic configuration; (__ · __) $|\underline{2p}3d^9\underline{L}\rangle$ final electronic configuration.

have simulated the spectra by two lines taking the energies, linewidths, and intensities as fitted parameters as well as the admixture of Lorentzian and Gaussian shapes to take into account the distortion due to the experimental line.

The spectrum of the bismuth cuprate $Bi_{1.9}Pb_{0.1}Sr_2Ca_{0.9}Y_{0.1}Cu_2O_{8+\delta}$ shows the agreement between experimental and simulated curves and the intensity distribution between both lines (Fig. 9, inset). The results of the simulation (Table I) show that the energy shift of the $|3d^9\underline{L}\rangle$ transition is constant throughout this series and smaller than for the $La_2Li_{0.5}Cu_{0.5}O_{3.96}$ compounds ($\varepsilon = 2.3$ eV).

The linewidths of the $|3d^9\underline{L}\rangle$ one appear always larger than the $|3d^9\rangle$ linewidth as expected. This is consistant with the idea that the energy of the $|3d^{10}\underline{L}\rangle$ configuration in the final state of the transition is broadened by the convolution of the width of the *d*-like band and the width of the midgap band. The $|3d^9\underline{L}\rangle$ linewidths have been kept constant in all simulations.

3. *Hole Density Estimation*

To estimate the hole density using the ratio

$$n_h = \frac{I_{|3d^9\underline{L}\rangle}}{I_{|3d^9\underline{L}\rangle} + I_{|3d^9\rangle}},$$

one has to take into account the anisotropic distribution of these hole carriers. In the bismuth layered cuprate of the 2212 type, it has been shown by EELS (*21*) at the oxygen *K*-edge that the holes are introduced only in the oxygen $2p_{x,y}$ orbitals and are completely absent from the $2p_z$ orbitals. This result is in agreement with the copper L_3-edge spectra realized on thin films or single crystals by Bianconi and co-workers (*23, 24, 33, 34*): from a recent and thorough investigation of Bi (2212) single crystals, these authors have shown that, at the copper L_3-edge, the intensity along the *z*-axis, about 20% of that in the (*a*,*b*) plane, contains a contribution due to $2p_{x,y}$ doping holes by the overlap with the copper $3d_{z^2}$ · atomic orbitals. With the electric field of the X-ray beam in the (*a*,*b*) plane of the structure, the $|3d^9\underline{L}\rangle$ transition appears clearly on the high energy side of the main peak whereas, with the electric field nearly parallel (±15°) to the *c*-axis of the structure, the $|3d^9\underline{L}\rangle$ does not appear any more and the total intensity is reduced to 25% of the former.

To confirm this angular dependence, we have recorded the copper L_3-edge spectra of an orientated polycrystalline thin film of $Bi_2Sr_2CaCu_2O_{8+\delta}$ (*c* axis perpendicular to the film plane), realized and characterized by Poullain and co-workers (*31*), for three orientations of the film plane with respect to the electrical field of the polarized incident beam (Fig. 10a). These spectra show the decrease of both the intensities of the main $|3d^9\rangle$ and of the $|3d^9\underline{L}\rangle$ lines, the latter disappearing for angles larger than 75°. Table I reports ratios

$$n_h = \frac{I_{|3d^9\underline{L}\rangle}}{I_{|3d^9\underline{L}\rangle} + I_{|3d^9\rangle}}.$$

It shows that n_h (35°) = 0.85 · n_h(0°), in accordance with the hole location restricted to the $3d_{x^2-y^2}$ copper orbital. More generally, if the electrical field direction is set at an angle Θ from the (*a*,*b*) plane, the $|3d^9\underline{L}\rangle$ intensities are given by $I_{|3d^9\underline{L}\rangle}(\Theta) = I_{|3d^9\underline{L}\rangle}(0°) \cdot \cos^2(\Theta)$ according to the dipole approximation, whereas the $|3d^9\rangle$ intensities are given by $I_{|3d^9\rangle} = I_{|3d^9\perp c\rangle} \cdot \cos^2(\theta) + I_{|3d^9\parallel c\rangle} \cdot \sin^2(\theta)$ with $I_{|3d^9\parallel c\rangle} \approx 0.2 I_{|3d^9\perp c\rangle}$.

The powder spectrum must correspond to the sample at 35° with respect to the electric field (magic angle). This result can be checked in Fig. 10b which shows, superposed for comparison, the Cu L_3-edges of the $Bi_2Sr_2CaCu_2O_8$ powder, used in this work, and of a Bi 2212 thin film recorded at 35° from the normal incidence. Owing for this correction, the final doping hole content per copper

$$n_{x,y} = \frac{I_{|3d^9\underline{L}\rangle} \cdot \cos^2(\theta)}{I_{|3d^9\underline{L}\rangle} \cdot \cos^2(\theta) + (I_{|3d^9\perp c\rangle} \cdot \cos^2(\theta) + I_{|3d^9\parallel c\rangle} \cdot \sin^2(\theta))}$$

can be calculated as shown in Table I.

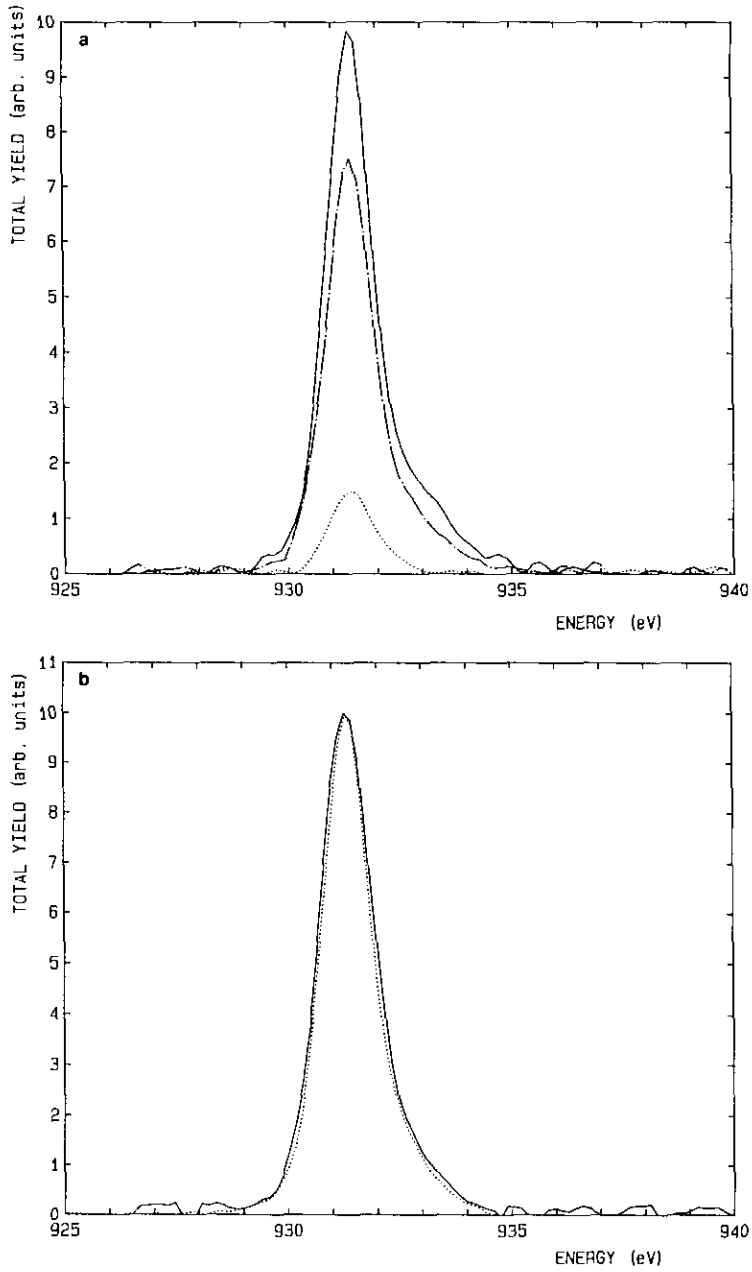

FIG. 10. Copper L_3-edge of an orientated (c-axis $\perp$ to the surface) $Bi_2Sr_2CaCu_2O_{8+\delta}$ thin film giving evidence of the angular dependence of the intensities of $|3d^9\rangle$ and $|3d^9\underline{L}\rangle$ electronic configurations. (a) Spectra corresponding to three different values of the angle between the film plane and the electrical field of the polarized incident beam: (———) 0°; (— · —) 35°; (· · ·) 75°. (b) Normalized spectra of the sinter $Bi_2Sr_2CaCu_2O_{8+\delta}$ (———) and of a linear combination $I_{//(a,b)} \cdot \cos(35°) + I_{//c} \cdot \sin(35°)$ (· · ·) of spectra recorded on the oriented thin film: $I_{//(a,b)}$corresponds to the electrical field of the incident beam in the (a,b) plane and $I_{//c}$ to the electrical field parallel to the c-axis.

D. Critical Temperatures and Density of Holes

Magnetic susceptibilities for the substituted compounds are plotted in Fig. 1. These curves show no significant evolution for $x \leq 0.1$, whereas a decrease of T_c's can be observed with increasing substitution rate. Critical temperatures have been reported in Table I. Diamagnetic volumes remain high (>70%) for $x \leq 0.3$ and decrease sharply above that value to vanish for $x > 0.75$.

For $0 \leq x \leq 0.3$, in the $Bi_{2-x}Pb_xCa_{1-x}Y_xCu_2O_{8+\delta}$ series. T_c's decrease continuously and smoothly when x increases. In such a case, electron microscopy has shown the existence of modulated structures in the whole microcrystals as in the parent compound $Bi_2Sr_2CaCu_2O_{8+\delta}$ (*30*). The existence of a solid state solution can be deduced from this observation for $x \leq 0.3$.

For $x \geq 0.75$ no more diamagnetic volume and T_c's can be observed and electron microscopy shows no more modulated structures. Here also the homogeneity of the electron micrographs can be interpreted on the basis of a solid state solution for $0.75 \leq x \leq 1$.

For $0.3 < x < 0.75$, in the range where T_c's and diamagnetic volumes decrease sharply with x, electron micrographs show inside each microcrystal the coexistence of domains a few hundred Å wide with modulated structures (arrowed in Fig. 11) and domains without modulations. The corresponding electron diffraction pattern (Fig. 10, inset) clearly exhibits the extra reflections associated with the modulations but weaker than in the $Bi_2Sr_2CaCu_2O_{2+\delta}$ parent compound, in agreement with the reduction of the modulated volume. A segregation between the superconducting and modulated bismuth-rich phase and the nonsuperconducting nonmodulated lead-rich one probably occurs in this substitution range and accounts for the sharp decrease of superconducting properties.

Increasing simultaneously the lead and the yttrium content, one can see (Fig. 9) the decrease of the $|3d^9\underline{L}\rangle$ contribution. For the $x = 0.75$ compound, the $|3d^9\underline{L}\rangle$ configuration does not appear any more and only a small broadening of the main line is still visible: this shows that the density of doping holes for this composition is less than 3%, which is the uncertainty of our evaluation. From $x = 0$ to $x = 0.5$, the calculated densities of holes decrease with x as T_c decreases (Table I). This confirms the correlation between T_c and hole density in the (a,b) plane of the layered superconductors, as already shown by XAS in thallium cuprates (*13*). The two compositions corresponding to $x = 0$ and $x = 0.1$ have approximately the same T_c's and, as expected, the hole densities $n_{x,y}$ are similar. Thus an optimum of T_c's around 85 K seems to occur for a hole density value $n_{x,y}$ close to 0.17 ± 0.03 as in thallium cuprates.

IV. Discussion

In the $Bi_{2-x}Pb_xCa_{1-x}Y_xCu_2O_{8+\delta}$ ($0 \leq x \leq 1$) series, in which a double substitution of Bi(III) by Pb(II) and Ca(II) by Y(III) has been realized, the copper valence state should be kept unchanged following the given valence states of the other elements and provided the oxygen stoichiometry remains constant. Due to electron (hole) transfer between Bi, Pb, and Cu ions, a continuous decrease of the hole density is achieved, in agreement with the simultaneous decrease of T_c's.

As in nonsubstituted 2212, we suppose that the hole doping of $[Cu–P_2]_\infty$ planes is realized through a charge transfer of electrons from $[Cu–O_2]_\infty$ planes to $[Bi–O]_\infty$ planes, acting as an electron reservoir. One has to bear in mind that the partially reduced valence of bismuth, observed on the Bi L_3-edges, can be obtained by a delocalization of extra electrons in the $[Bi–O]_\infty$ planes in a band based on the overlapping of Bi $6s$, and $6p_{x,y}$ and O $2p_{x,y}$ orbitals.

To account for the presence of a mixed valence of lead, one can think also of electron transfer between lead and copper and/or lead and bismuth. Based on the solid state

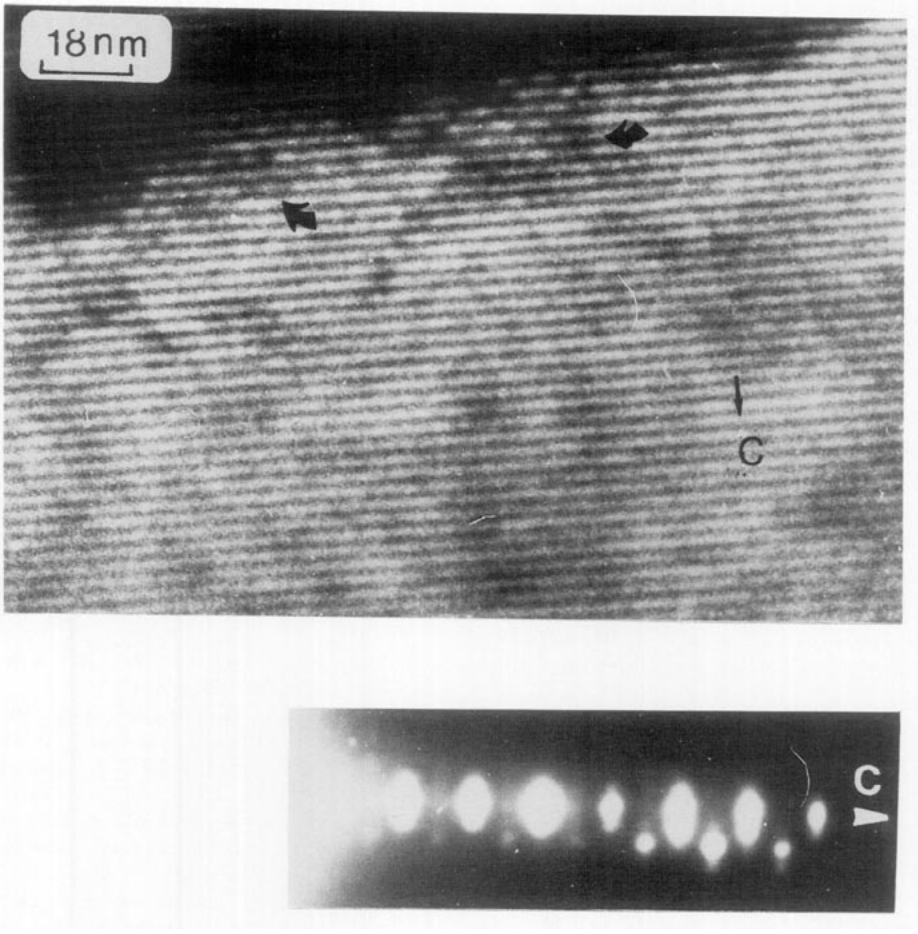

FIG. 11. Electron micrography of a $Bi_{1.5}Pb_{0.5}Sr_2Ca_{0.5}Y_{0.5}Cu_2O_{8+\delta}$ crystal showing the modulated structures characteristic of the Bi(2212) phase in small domains (arrows) and confirmed by the presence of weak superstructure reflections in the corresponding diffraction pattern.

chemistry of compounds containing lead and copper, the first electron transfer occurs from lead to copper and can account for the decrease of the hole density when the substitution amount x increases.

The second electron transfer takes place from lead to bismuth inside the $[Bi–O]_\infty$ planes. To realize such a transfer, the top of the lead 6*s* level should be above the bismuth 6*s* one: This can be realized, at least at a low substitution rate x, by the strong crystal field created by oxygens around Pb(IV) cations, which should act as deep donor levels for the Bi–O band.

When x increases, the excess electrons given to the structure by the Y^{3+} cations can be absorbed by the lead 6*s* orbitals such that lead tends to Pb(II), whereas the lead 6*s* and 6*p* orbitals overlapping with the O $2p_{x,y}$ contributes to the conduction band in the $[(Bi,Pb)O]_\infty$ planes.

But, for $0.3 \leq x < 0.7$, the quick decrease of T_c's and diamagnetic volumes is most likely due to segregation between a high T_c bismuth-rich phase ($x = 0.25$) and a nonsuperconducting lead-rich phase ($x = 0.75$) whose relative amounts change with x.

V. Concluding Remarks

This XAS study of the $Bi_{2-x}Pb_xCa_{1-x}Y_xCu_2O_{8+\delta}$ ($0 \leq x \leq 1$) series at Bi, Pb, and

Cu L_3-edges has shown the simultaneous presence of mixed valence states of bismuth, lead, and copper. Electron (hole) transfer can be proposed between Bi and Pb in the $[Bi–O]_\infty$ planes and with Cu in the $[CuO_2]_\infty$ planes to account for the variation of the density of holes.

An estimation of the hole density in the $[CuO_2]_\infty$ planes has been performed by measuring the relative intensity of the $|3d^9\underline{L}\rangle$ configuration on the copper L_3-edges. The hole densities decrease when x increases which leads to the decrease of critical temperatures from 85 K to no superconductivity.

A comparison of these results with the microstructure as observed by electron microscopy led to the conclusion that two solid state solutions, superconducting for $0 \leq x \leq 0.3$ and not for $0.75 \leq x \leq 1$, are separated by a domain of phasoids of the limit compositions.

References

1. A. Q. Pham, A. Maignan, M. Hervieu, C. Michel, and B. Raveau, *Physica C* **191,** 77 (1992).
2. A. Bianconi, J. Budnick, A. M. Flank, A. Fontaine, P. Lagarde, A. Marcelli, H. Tolentino, B. Chamberland, G. Demazeau, C. Michel, and B. Raveau, *Phys. Lett. A* **127,** 285 (1988).
3. E. E. Alp, G. K. Shenoy, D. G. Hinks, D. W. Capone II, L. Soderholm, H. B. Schuttler, J. Guo, D. Ellis, P. A. Montano, and M. Ramanathan, *Phys. Rev. B* **35,** 13, 7199 (1987).
4. F. Baudelet, G. Collin, E. Dartyge, A. Fontaine, J. P. Kappler, G. Krill, J. P. Itie, J. Jegoudez, M. Maurer, Ph. Monod, A. Revcolevski, H. Tolentino, G. Tourillon, and M. Verdaguer, *Z. Phys. B* **69,** 141 (1988).
5. A. Bianconi, A. Clozza, A. Castellano, S. Dellalonga, M. De Santis, A. Dicicco, K. Garg, P. Delocv, A. Gargano, R. Giorgi, P. Lagarde, A. M. Flank, and A. Marcelli, *J. Phys. C* **9,** 1179 (1988).
6. T. Gourieux, G. Krill, M. Maurier, M. F. Ravet, A. Menny, H. Tolentino, and A. Fontaine, *Phys. Rev. B* **37,** 7516 (1988).
7. H. Tolentino, A. Fontaine, A. M. Flank, P. Lagarde, J. Y. Henry, J. Rossat-Mignod, T. Gourieux, G. Krill, and F. Studer, *in* "IWEPS '90" (I. Fink, Ed.), Springer Series of Solid State Sciences, Springer-Verlag, Berlin, New York, in press.
8. B. Raveau, C. Michel, M. Hervieu, J. Provost, and F. Studer, *in* "Earlier and Recent Aspects of Superconductivity" (J. G. Bednorz and K. A. Müller, Eds.), Solid State Sciences, Vol. 90, pp. 66–95.
9. R. Retoux, F. Studer, C. Michel, B. Raveau, A. Fontaine, and E. Dartyge, *Phys. Rev. B* **41,** 193 (1990).
10. F. Studer, D. Bourgault, C. Martin, R. Retoux, C. Michel, and B. Raveau, *Physica C* **159,** 609 (1990).
11. F. Studer, N. Merrien, C. Martin, C. Michel, and B. Raveau, *Physica C* **178,** 324 (1991).
12. H. Tolentino, A. Fontaine, F. Baudelet, T. Gourieux, G. Krill, J-Y Henry, and J. Rossat-Mignod, submitted for publication.
13. N. Merrien, F. Studer, A. Maignan, C. Martin, C. Michel, B. Raveau, and A. M. Flank, *J. Solid State Chem.*, in press.
14. A. Fujimori, E. Takayama-Muromachi, Y. Uchida, and B. Okai, *Phys. Rev. B* **35,** 8814 (1987).
15. J. Zaanen, G. A. Sawatzky, and J. W. Allen, *Phys. Rev. Lett.* **55,** 418 (1985).
16. A. Bianconi, A. Congiu-Castellano, M. de Santis, P. Rudolf, P. Lagarde, A. M. Flank, and A. Marcelli, *Solid State Commun.* **63,** 11, 1009 (1987).
17. A. Bianconi, A. Congiu-Castellano, M. de Santis, P. Delogu, A. Gargano, and R. Giorgi, *Solid State Commun.* **63,** 12, 1135 (1987).
18. P. Kuiper, G. Kruizinga, J. Ghusen, G. A. Sawatzky, and H. Verweij, *Phys. Rev. Lett.* **62,** 2, 221 (1989).
19. T. Chen, F. Sette, Y. Ma, M. S. Hybertsen, E. B. Stechel, W. M. C. Foulkes, M. Schluter, S-W. Cheong, A. S. Cooper, L. W. Rupp, B. Batlogg, Y. L. Soo, Z. H. Ming, A. Krol, and Y. H. Kao, *Phys. Rev. Lett.* **66,** 1, 104 (1991).
20. J. Fink, J. Pflüger, Th. Müller-Heinzerling, N. Nücker, B. Scheerer, H. Romberg, M. Alexander, R. Manzke, T. Buslaps, R. Claessen, and M. Skibowski *in* "Earlier and Recent Aspects of Superconductivity" (K. A. Müller and G. Berdnoz, Eds.), Proceedings of the International School of Materials Science and Technology, Erice, July 1989.
21. J. Fink, N. Nücker, H. Romberg, M. Alexander, and P. Adelman, *in* "Highlights of the Eighties and Future Prospects in Condensed Matter Physics," Proceedings of a NATO Science Forum, Biarritz, France, Sept. 16–21, 1990.
22. A. Krol, C. S. Lin, Z. H. Ming, C. J. Sher, Y. H. Kao, C. T. Chen, F. Sette, Y. Ma, G. C. Smith, Y. Z. Zhu, and D. T. Shaw, *Phys. Rev. B* **42,** 4 2635 (1990).

23. A. Bianconi, M. De Santis, A. Di Cicco, A. M. Flank, A. Fontaine, P. Lagarde, H. Katayama-Yoshida, A. Kotani, and A. Marcelli, *Phys. Rev. B* **38,** 10, 7196 (1988).
24. A. M. Flank, P. Lagarde, A. Bianconi, P. Castrucci, A. Fabrizi, M. Pompa, H. Katayama-Yoshida, and G. Calestani, *in* "Proceedings of the Ninth International Conference on Vacuum Ultraviolet Radiation Physics, Honolulu, July 17–21, 1989, *Phys. Script.* **41,** 901 (1990).
25. F. Herman, R. V. Kasowski, and W. Y. Hsu, *Phys. Rev. B* **38,** 1, 204 (1988).
26. F. C. Zhang and T. M. Rice, *Phys. Rev. B* **37,** 3759 (1988).
27. N. Nücker, H. Romberg, X. X. Xi, J. Fink, B. Gegenheimer, and Z. X. Zhao, *Phys. Rev. B* **39,** 10, 6619 (1989).
28. J. P. Attfield and G. Férey, *J. Solid State Chem.* **80,** 112 (1989).
29. R. Retoux, V. Caignaert, J. Provost, C. Michel, M. Hervieu, and B. Raveau, *J. Solid State Chem.* **79,** 157 (1989).
30. P. Lejay, P. de Rango, A. Sulpice, B. Giordanengo, R. Tournier, R. Retoux, F. Deslandes, C. Michel, M. Hervieu, and B. Raveau, *Rev. Phys. Appl.* **24,** 485 (1989).
31. T. Brousse, G. Poullain, J. F. Hamet, H. Murray, and B. Raveau, *Physica C* **170,** 545 (1990).
32. A. Bianconi, E. Fritsch, G. Calas, and J. Petiau, *Phys. Rev. B* **32,** 4292 (1985).
33. A. Bianconi, S. Della Longa, C. Li, M. Pompa, A. Congiu-Castellano, D. Udron, A. M. Flank, and P. Lagarde, *Phys. Rev. B* **44,** 18, 10,126 (1991).
34. A. Bianconi, Ch. Li, S. Della Longa, and M. Pompa, *Phys. Rev. B* **45,** 9, 4989 (1992).
35. H. Tolentino, A. Fontaine, A. M. Flank, P. Lagarde, and F. Studer, *Physica C* **179,** 387 (1991).
36. G. Demazeau, C. Parent, M. Pouchard, and P. Hagenmuller, *Mater. Res. Bull.* **7,** 913 (1972).
37. K. J. Rao and J. Wong, *J. Chem. Phys.* **81,** 11, 4832 (1984).